IOP Publishing

Semiconductor Science and Technology

Semicond. Sci. Technol. **39** (2024) 065007 (5pp)

https://doi.org/10.1088/1361-6641/ad40c7

Electronic signal for mechanical failure in two-dimensional *g*-SiC

Jing Li[1], Tan Shi[1,*], Chenyang Lu[1] and Qing Peng[2,3,4,*]

[1] School of Nuclear Science and Technology, Xi'an Jiaotong University, Xi'an 710049, People's Republic of China

[2] State Key Laboratory of Nonlinear Mechanics, Institute of Mechanics, Chinese Academy of Sciences, Beijing 100190, People's Republic of China

[3] Center of Materials Science and Optoelectronics Engineering, University of Chinese Academy of Sciences, Beijing 100049, People's Republic of China

[4] Guangdong Aerospace Research Academy, Guangzhou 511458, People's Republic of China

E-mail: tan.shi0122@xjtu.edu.cn and pengqing@imech.ac.cn

Received 21 January 2024, revised 6 April 2024
Accepted for publication 19 April 2024
Published 30 April 2024

Abstract

It is non-trivial to identify mechanical failure using first-principles calculations as only long-wave phonons are used in these models due to size limitations. Here, we propose a new criterion to predict the mechanical failure by electronic bandgap closure in graphene-like two-dimensional silicon carbide (*g*-SiC) monolayer. The electronic bandgap decreases with strain and closes beyond the ultimate strain. This mechano-electronic coupling suggests that the onset of the zero bandgap and the correlation between electronic bandgap and ultimate strain could be used to predict the ideal mechanical failure of *g*-SiC monolayers.

Keywords: instability, mechanical properties, electronic properties, two-dimensional SiC, first-principles calculations, mechanical failure

The monolayer silicon carbide (SiC), similar to graphene, is a two-dimensional material comprising a single atomic layer arranged in a hexagonal lattice structure. Stability predictions for this material indicate the presence of indirect bandgaps, calculated to be approximately 2.55 eV [1]. The presence of this bandgap confers a significant advantage in the development of optoelectronic devices [1–3]. The material also demonstrates potential for integration in a wide range of applications, including field-effect transistors, sensors, nanoelectromechanical systems, supercapacitors, etc. Ultra-thin 2D-SiC films have been fabricated by solution exfoliation [4]. Very recently, monolayer SiC has also been fabricated using a wet exfoliation method and has shown to be environmentally stable [5]. The obtained two-dimensional SiC exhibits visible-light emission, confirming its potential applications for electronics and optoelectronics [5]. A considerable amount of theoretical work has been conducted to investigate its structural stability, thermodynamic stability, as well as its electronic and optoelectronic properties [2, 6–9]. For instance, the SiC monolayer has been identified as the most thermodynamically stable structure among over a wide range of Si_xC_{1-x} structures based on first-principles calculations [10]. However, its mechanical stability and mechanical properties attract comparatively less attention. Its non-linear mechanical behavior has only been explored recently [11].

It has been predicted that the transition of the SiC nanosheet from an indirect to a direct bandgap can be modulated by altering the lattice constant [2]. Recent reports also indicate that strain engineering can be used to manipulate the electronic and optical properties of two-dimensional SiC [12]. The mechanical properties of the *g*-SiC monolayer has been investigated by first-principles calculations in the meta-GGA level by authors [13]. However, the correlation between the mechanical behaviors and the electronic band structure behaviors in response to the strains is still elusive. This letter aims to investigate the relationship between the nonlinear mechanical behaviors of *g*-SiC under large strains and the electronic bandgaps, and establish criterion for mechanical failure based on Density functional theory (DFT) calculations.

* Authors to whom any correspondence should be addressed.

© 2024 IOP Publishing Ltd

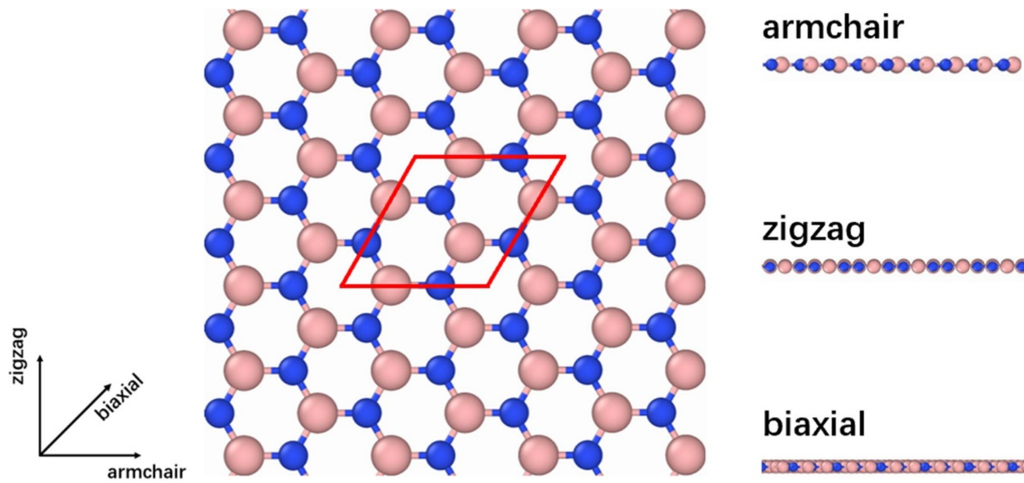

Figure 1. Geometry. The graphene-like planar structure of *g*-SiC is displayed in the figure, including views from the top, along with armchair, zigzag, and biaxial deformation directions. The red contour represents the simulated supercell of six atoms.

DFT calculations were performed with the Vienna Ab-initio Simulation Package (VASP) [14–16]. We consider an unit cell of 6 atoms (3 C + 3 Si atoms) with periodic boundary conditions with a vacuum thickness of 15 Å (see figure 1). The selection of a 6-atom unit cell instead of a 2-atom unit cell is predicated on the presence of a soft mode that leads to mechanical instability [17]. In this study, we employed the Perdew–Burke–Ernzerhof generalized gradient approximation (PBE-GGA) [18] and the strongly constrained and appropriately normed meta-generalized gradient approximation (SCAN-mGGA) [19] for exchange-correlation functionals in the DFT calculations. The electrons explicitly included are the $2s^2 2p^2$ and $3s^2 3p^2$ electrons for carbon and silicon atoms, respectively. A $24 \times 24 \times 1$ *k*-mesh is adopted. The plane-wave cutoff is set to 600 eV. The electronic loop convergence criterion is 10^{-6} eV. The optimized structure is determined by minimization of Hellmann–Feynman forces with a threshold of 0.001 eV Å^{-1}. The system energies, atomic forces and stresses are determined under various deformation configurations and the corresponding stress–strain relationships are obtained.

In order to obtain the stress–strain relationships, the following deformation states are considered: uni-axial strain in the armchair direction (the direction to the nearest neighbor, denoted as *mode a*); uni-axial strain in the zigzag direction (the direction to the second nearest neighbor, denoted as *mode z*); and equibiaxial strain (denoted as *mode b*). These directions are depicted in figure 1. Due to the large mechanical loading, all deformations are quantified using the Lagrangian strain, which is defined as $\eta = (F^T F - I)/2$, where F is the deformation gradient tensor and I is the identity tensor. The Lagrangian strain varies from -0.10 to 0.40 with a step size of 0.01 applied across all selected modes of deformation. To accommodate to the two-dimensional nature of the structure and avoid uncertainty on the structure thickness, we use the second Piola–Kirchhoff (P-K) stress [20] to express the forces per unit length (unit: N m^{-1}). High-order elastic tensors up to fifth order (fifth-order elastic constants: $C_{\mathrm{ijklmnopqr}}$) are used to determine the elastic constants. Since the structure has a point group of D_{3h}, only 14 independent elastic constants need to be calculated due to the symmetric operations. These 14 elastic constants are calculated by a least-squares fitting approach, utilizing stress–strain data derived from DFT calculations, as described in our previous work [21]. This method takes into account the 2D nature of the structure and has been extensively used to study the mechanical properties of 2D materials [22–24]. By expressing the stress–strain response in the tensor form for the three deformation directions, least-square solution to linear equations related to elastic constants of different orders (up to fifth order) are then determined, which can be used to study the elastic mechanical properties in both the linear and nonlinear regime. In addition to *g*-SiC, we also compared this new compound material with its 'parents', graphene and silicene. We have also studied the electronic structures under various mechanical loadings in the armchair, zigzag and equibiaxial direction. Both positive (for elongation) and negative (for compression) strains are examined. When the strains are applied to the system, all the atoms are allowed full freedom of motion.

The lattice constant of *g*-SiC from geometry optimization is $a = 3.10$ Å, which is consistent with previous DFT results and the bulk 4H-SiC ($a = 3.08$ Å) [25]. The atomic structure is similar to that of graphene, which is purely two-dimensional (see figure 1). The bond length between nearest carbon and silicon is 1.79 Å. Overall, our findings regarding the atomic structure of *g*-SiC are consistent with previous results obtained from DFT calculations [1, 2, 26, 27].

In order to obtain the ultimate strain and strength, first, the second P-K stress [21] as a function of the Lagrangian strain for the aforementioned strain directions is determined. The second P-K stress is converted from the Cauchy stress obtained from DFT calculations based on the deformation gradient tensor. Next, the ultimate strength (Σ_u) and ultimate strain (η_u) are determined based on the stress–strain results, compared with that of graphene and silicene (see figure 2) [13, 22, 28]. The ultimate strength is defined as the highest stress

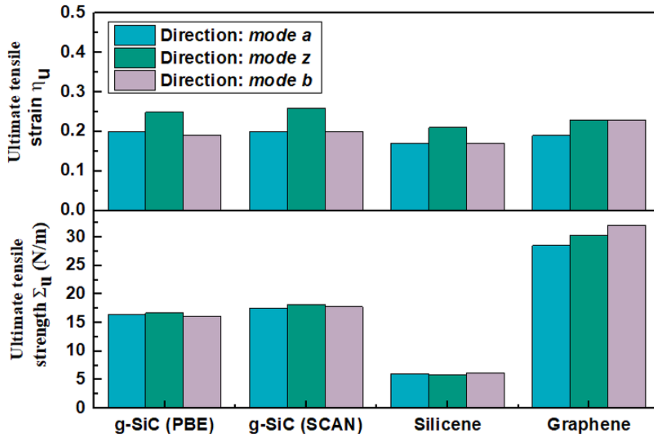

Figure 2. Critical strains and strengths. Ultimate tensile strains of η_u^a, η_u^z, and η_u^b and ultimate tensile strengths of Σ_u^a, Σ_u^x and Σ_u^b for mode *a*, *z*, *b* from SCAN and PBE calculations in *g*-SiC, where data from silicene and graphene were also included for comparison.

it can endure during stretching, and the strain at which this occurs is termed the ultimate strain. Although critical mechanical properties have been calculated previously in *g*-SiC [13], to our knowledge, it is the first time that they are used to correlate with bandgaps in two-dimensional materials for mechanical failure prediction, which is also a necessary step to establish such a correlation. As the strain increases, the carbon-silicon (C-Si) bonds elongate and ultimately lead to rupture. We note that the pristine *g*-SiC systems, when subjected to strains exceeding their ultimate strains, enter a meta-stable state. This state is susceptible to destabilization by factors such as long wavelength perturbations, crystal defects, and high thermal effect. It is found that the material exhibits asymmetric behavior under compressive and tensile strains. For the armchair deformation mode, the bonds oriented parallel to the strain direction undergo more severe stretching compared to those in other orientations. As shown in figure 2, the η_u in armchair direction is 0.2, larger than silicene (0.17) and graphene (0.19). In the case of zigzag deformation, there are no bonds oriented parallel to this direction. Instead, the bonds incline at an angle of 30° to the zigzag direction and these bonds experience more severe stretching than those in the armchair direction. The η_u values in this zigzag direction with the SCAN and PBE functionals are 0.26 and 0.25, respectively, also larger than that of both silicene and graphene. At the ultimate strain, it is shown that the bonds inclined towards the armchair direction undergo rupture. Under the biaxial deformation, the ultimate strains with the SCAN and PBE functionals are $\eta_u^b = 0.20$ and 0.19, respectively, where all the C-Si bonds are ruptured. Our results show that the *g*-SiC monolayer exhibits greater flexibility compared to both graphene and silicene. The ultimate tensile strength results are also presented in figure 2. It can be seen that the among different deformation directions, Σ_u values are very close. As planar strength is shown here, we note that it is also possible to convert to conventional unit of in-plane stiffness (GPa) by adopting an interlayer van der Waals distance (3.75 Å in the case of *g*-SiC [12]).

In addition to the mechanical properties, we have studied the electronic bandgaps under various mechanical loading conditions. The electronic bandgaps of monolayer *g*-SiC are attributed to the overlap of atomic orbitals and electron charge distribution. In principle, the mechanical strain changes the bond lengths and electronic charge distribution, which ultimately affects the bandgap. Therefore, strain is a crucial factor in tuning the electronic properties. Our results of bandgaps as a function of strains are illustrated in figure 3(a). At zero strain, the electronic bandgap is 2.57 eV, in an excellent agreement with previous DFT calculations [1, 8, 26, 29]. All the tensile strains decrease the bandgaps. The rates of the decrease are similar among the three modes when the strain is smaller than 0.05. There are considerable differences when the strain is larger than 0.1. When the strain is beyond a critical value, the bandgap becomes zero, which corresponds to the isolated atom state.

We denote this critical strain as zero-bandgap strain, which is the minimum strain required to close up the electronic bandgap. The zero bandgap therefore is a clear sign of the broken chemical bonds into individual atoms. The zero-bandgap strains are $\eta_e^a = 0.27$, $\eta_e^z = 0.25$, and $\eta_e^b = 0.19$ for uniaxial armchair, uniaxial zigzag, and biaxial deformation, respectively. Recall that the ultimate tensile strains are 0.20, 0.25, and 0.19, respectively. The zero-bandgap strain is equal to ultimate tensile strain for uniaxial zigzag and biaxial deformation. The zero-bandgap strain is 0.07 larger than the ultimate tensile strain in uniaxial armchair deformation. Therefore, the zero-bandgap strain is useful to quantitatively estimate the failure strain of *g*-SiC, as shown in figure 4. We note that even though the bandgap closing strain and ultimate tensile strain do not correspond exactly in numerical values in all cases, the broader significance of this research lies in unveiling the strong correlation between these two physical quantities. This could be understood as with the increment of the bond length of Si-C under tensile strain, the overlap of the atomic orbitals becomes lessens. When the chemical bond of Si-C is dissociated, the overlap of the atomic orbitals disappears. All the atoms in the system are in isolated individual atomic state. The bonding-antibonding states caused by the overlap of atomic orbitals now restore to the original atomic states. As a result, the bandgap of the system approaches to zero. It is worth noting that the PBE-GGA functionals we used cannot accurately predict the bandgaps due to the inherent limitation in accurately describing discontinuous energy in the exchange-correlation potential. However, the trend in the bandgap can be precisely characterized in relation to mechanical loading. To confirm that, we applied state-of-the-art 'SCAN' [19, 30], a meta-generalized-gradient approximation of the exchange-correlation functional of the electronic charge density, to compute the bandgaps, as shown in solid lines in figure 3(a). The corresponding results of density of states (see figure 3(b)) also confirm the variation in bandgap with varying strains. Clearly, the trend of bandgaps with strains is similar to that from PBE-GGA calculations.

When the compressive strains are applied, the electronic bandgaps have more complex behaviors than tensile strains. The biaxial compressive strains enlarge the electronic

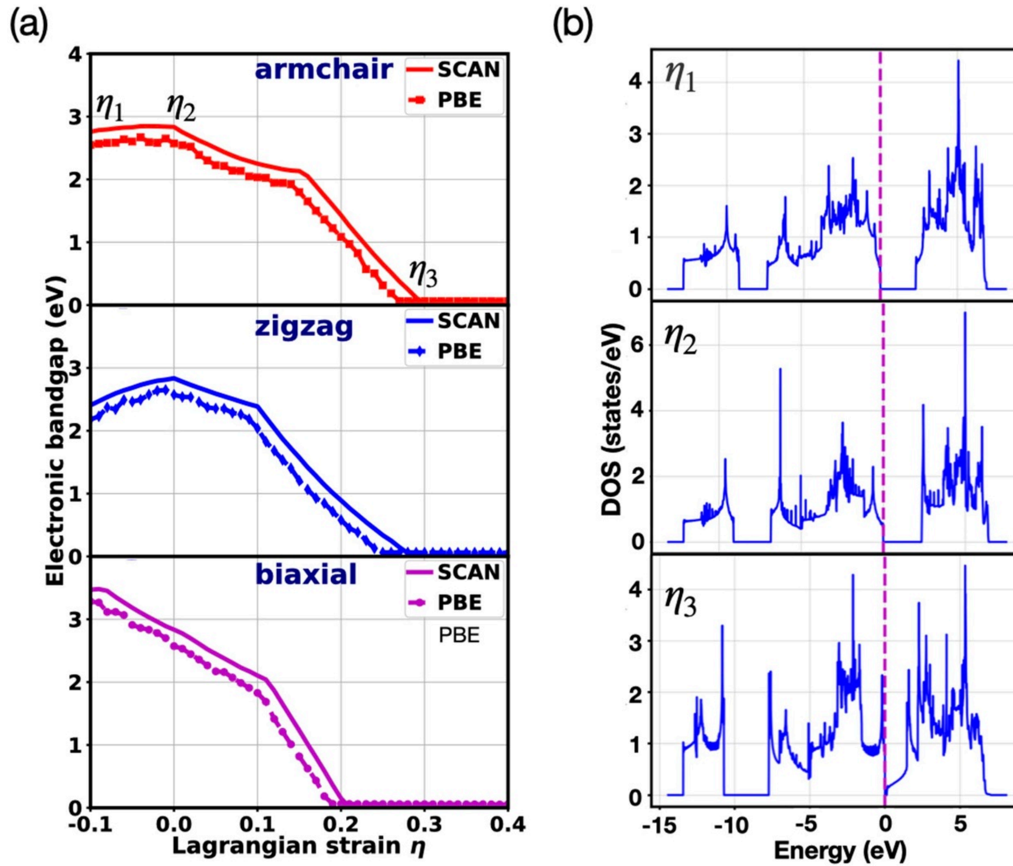

Figure 3. Response of electronic bandgap to strain. (a) Electronic bandgap as a function of strain along the armchair, zigzag, and biaxial directions. Zero bandgap indicates isolated individual atomic state. (b) Representative density of states at strains labeled in (a) for the armchair deformation with the SCAN functional.

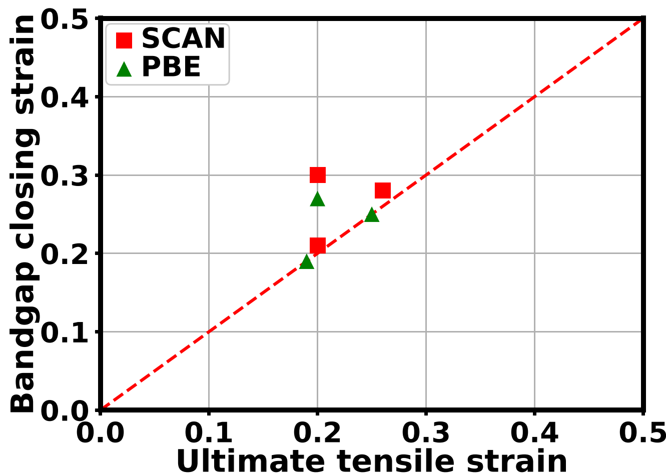

Figure 4. Correlation between bandgap closing strain and ultimate tensile strain. Comparison of the bandgap-closing strain to the ultimate tensile strain from both PBE and SCAN calculations.

bandgaps, contrary to the uniaxial strains along zigzag and armchair directions. The biaxial behavior can still be understood from the aspect of the electronegativity. However, the uniaxial strains affect the bond lengths to a different extent, making the variation of the bandgap more complicated. For example, the decrease of the electronic bandgap in zigzag compressive strain is much faster than that under armchair strains. The decrease of the electronic bandgap with the increase of biaxial strain can be approximately expressed as $E_g^b = 3.283 - 7.275\eta^b$ in the range of $-0.1 \leqslant \eta^b \leqslant 0.1$. This result provides a roadmap in bandgap engineering via mechanical strains.

Our striking finding is the correlation between the bandgap closure and the system mechanical failure, particularly along the armchair and zigzag directions. The coupling between the electronic bandgaps and the mechanical strain implies that the zero electronic bandgap could serve as an indicator for ideal mechanical failure of the system, which in general is difficult to identify in DFT calculations using small unit cells. The strain η_e corresponding to the closure of electronic bandgap η_e is an upper bound of ultimate tensile strain η_u, as $\eta_e \geqslant \eta_u$. Therefore, our results suggest a new routine to study the failure mechanism of *g*-SiC monolayers. Opposed to the classical method that one needs to have the stress–strain relationship *a priori* to judge the mechanical failure, this bandgap method relies on the correlation with the electronic bandgap, taking the advantage of mechano-electronic coupling. It is also of great interest to explore the relationship between

ultimate tensile strain and bandgap in other two-dimensional or three-dimensional materials to assess the applicability of this approach.

Data availability statement

The data cannot be made publicly available upon publication because the cost of preparing, depositing and hosting the data would be prohibitive within the terms of this research project. The data that support the findings of this study are available upon reasonable request from the authors.

Acknowledgments

The authors acknowledge the support from the National Natural Science Foundation of China (Grant Nos. 12105219 and 12272378), High-level Innovation Research Institute Program of Guangdong Province (Grant No. 2020B0909010003), and LiYing Program of the Institute of Mechanics, Chinese Academy of Sciences (Grant No. E1Z1011001).

Conflict of interest

The authors declare no competing financial interests.

ORCID iD

Qing Peng https://orcid.org/0000-0003-4122-5380

References

[1] Şahin H, Cahangirov S, Topsakal M, Bekaroglu E, Akturk E, Senger R T and Ciraci S 2009 *Phys. Rev.* B **80** 155453
[2] Lü T-Y, Liao X-X, Wang H-Q and Zheng J-C 2012 *J. Mater. Chem.* **22** 10062–8
[3] Ganguly G, De S C, Ray S and Barua A 1991 *J. Appl. Phys.* **69** 3915–23
[4] Lin S 2012 *J. Phys. Chem.* C **116** 3951–5
[5] Chabi S, Guler Z, Brearley A J, Benavidez A D and Luk T S 2021 *Nanomaterials* **11** 1799
[6] Wu R, Zhou K, Yue C Y, Wei J and Pan Y 2015 *Prog. Mater. Sci.* **72** 1–60
[7] Lin X, Lin S, Xu Y, Hakro A A, Hasan T, Zhang B, Yu B, Luo J, Li E and Chen H 2013 *J. Mater. Chem.* **1** 2131–5
[8] Hsueh H, Guo G and Louie S G 2011 *Phys. Rev.* B **84** 085404
[9] Wu I and Guo G 2007 *Phys. Rev.* B **76** 035343
[10] Shi Z, Zhang Z, Kutana A and Yakobson B I 2015 *ACS Nano* **9** 9802–9
[11] Peng Q 2020 *Mech. Mater.* **148** 103473
[12] Xu Z, Li Y and Liu Z 2016 *Mater. Des.* **108** 333–42
[13] Peng Q 2021 *Crystals* **11** 120
[14] Kresse G and Furthmüller J 1996 *Comput. Mater. Sci.* **6** 15–50
[15] Hohenberg P and Kohn W 1964 *Phys. Rev* **136** B864
[16] Kohn W and Sham L J 1965 *Phys. Rev.* **140** A1133
[17] Marianetti C A and Yevick H G 2010 *Phys. Rev. Lett.* **105** 245502
[18] Perdew J P, Burke K and Ernzerhof M 1996 *Phys. Rev. Lett.* **77** 3865
[19] Sun J, Ruzsinszky A and Perdew J P 2015 *Phys. Rev. Lett.* **115** 036402
[20] Peng Q, Zamiri A R, Ji W and De S 2012 *Acta Mech.* **223** 2591–6
[21] Peng Q, Ji W and De S 2012 *Comput. Mater. Sci.* **56** 11–17
[22] Peng Q, Liang C, Ji W and De S 2013 *Phys. Chem. Chem. Phys.* **15** 2003–11
[23] Peng Q, Liang C, Ji W and De S 2013 *Appl. Phys.* A **113** 483–90
[24] Peng Q, Chen Z and De S 2015 *Mech. Adv. Mater. Struct.* **22** 717–21
[25] Kamitani K, Grimsditch M, Nipko J, Loong C-K, Okada M and Kimura I 1997 *J. Appl. Phys.* **82** 3152–4
[26] Bekaroglu E, Topsakal M, Cahangirov S and Ciraci S 2010 *Phys. Rev.* B **81** 075433
[27] Wang N, Tian Y, Zhao J and Jin P 2016 *J. Mol. Graph. Modelling* **66** 196–200
[28] Peng Q, Wen X and De S 2013 *RSC Adv.* **3** 13772–81
[29] Sun L, Li Y, Li Z, Li Q, Zhou Z, Chen Z, Yang J and Hou J 2008 *J. Chem. Phys.* **129** 174114
[30] Sun J *et al* 2016 *Nat. Chem.* **8** 831–6